AFRL-SN-RS-TR-1999-174
In-House Report
February 2000

ULTRAVIOLET MEASUREMENT OF OPTICAL MEMORY SUBSYSTEMS

Joseph Osman, Rebecca Bussjager and David Grucza

APPROVED FOR PUBLIC RELEASE; DISTRIBUTION UNLIMITED.

AIR FORCE RESEARCH LABORATORY
SENSORS DIRECTORATE
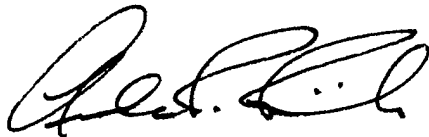**ROME RESEARCH SITE**
ROME, NEW YORK

20000308 015

Although this report references a limited document (*), listed on page 24, no limited information has been extracted.

This report has been reviewed by the Air Force Research Laboratory, Information Directorate, Public Affairs Office (IFOIPA) and is releasable to the National Technical Information Service (NTIS). At NTIS it will be releasable to the general public, including foreign nations.

AFRL-SN-RS-TR-1999-174 has been reviewed and is approved for publication.

APPROVED:

ANDREW R. PIRICH
Chief, Photonics Processing Branch
Sensors Directorate

FOR THE DIRECTOR:

ROBERT G. POLCE
Chief, Rome Operations Office
Sensors Directorate

If your address has changed or if you wish to be removed from the Air Force Research Laboratory Rome Research Site mailing list, or if the addressee is no longer employed by your organization, please notify AFRL/SNDP, 25 Electronic Parkway, Rome, NY 13441-4515. This will assist us in maintaining a current mailing list.

Do not return copies of this report unless contractual obligations or notices on a specific document require that it be returned.

REPORT DOCUMENTATION PAGE

1. AGENCY USE ONLY *(Leave blank)*	2. REPORT DATE	3. REPORT TYPE AND DATES COVERED
	February 2000	In-House Final, 11 Feb 97 - 11 Feb 98

4. TITLE AND SUBTITLE
ULTRAVIOLET MEASUREMENTS OF OPTICAL MEMORY SUBSYSTEMS

5. FUNDING NUMBERS
IN-HOUSE
PE - 61102F
PR - 2304
TA - 07
WU - 01

6. AUTHOR(S)
Joseph Osman, Rebecca Bussjager, David Grucza

7. PERFORMING ORGANIZATION NAME(S) AND ADDRESS(ES)
Air Force Research Laboratory/SNDP
25 Electronic Pky
Rome NY 13441-4515

8. PERFORMING ORGANIZATION REPORT NUMBER

AFRL-SN-RS-TR-1999-174

9. SPONSORING/MONITORING AGENCY NAME(S) AND ADDRESS(ES)
Air Force Research Laboratory/SNDP
25 Electronic Pky
Rome NY 13441-4515

10. SPONSORING/MONITORING AGENCY REPORT NUMBER

AFRL-SN-RS-TR-1999-174

11. SUPPLEMENTARY NOTES
Project Engineer: Joseph Osman, AFRL/SNDP, (315) 330-7671

12a. DISTRIBUTION AVAILABILITY STATEMENT
APPROVED FOR PUBLIC RELEASE: DISTRIBUTION UNLIMITED

12b. DISTRIBUTION CODE

13. ABSTRACT *(Maximum 200 words)*
This effort mapped out the wavelengths of the states within the bandgap which have enough absorption strength to be used to write the material. Since metal oxides are always highly defected materials, we predict that subbandgap light could also be used to drive other processes, such as catalysis, which were previously only thought to be possible with superbandgap light. We found that using 385 nm light lowered the threshold by a factor of about 1000 compared to blue-green wavelengths. We measured 100 ns write speed at 385 nm, which is close to the desired 50 ns write speed and measured 2.5 ns write from 400 to 700 nm. We showed that adding a layer of TiO_2 lowered the threshold by a factor of 1/3. So doping and adding other materials should be investigated. We also showed that writing was possible by preheating the material with IR before applying light in the UV to blue-green range. So the two wavelength beams will not have to be strictly coaxial when writing the material, relaxing the requirements for a write head in a disk drive. We conclusively proved that the IR light acts only as heat.

14. SUBJECT TERMS
optical memory, optical storage, tungsten oxide, titanium oxide, transition metal oxide, thin films, sol-gels, Raman spectroscopy, catalysis

15. NUMBER OF PAGES
32

16. PRICE CODE

17. SECURITY CLASSIFICATION OF REPORT	18. SECURITY CLASSIFICATION OF THIS PAGE	19. SECURITY CLASSIFICATION OF ABSTRACT	20. LIMITATION OF ABSTRACT
UNCLASSIFIED	UNCLASSIFIED	UNCLASSIFIED	UNL

Table of Contents

List of Figures

1 Introduction

1.1 General Introduction

Systems requirements for projected future AF radar and intelligence signal processing systems include large capacity, high speed memory storage. The use of optics provides both speed and density advantages over electronic approaches. Optical transitions can be very fast, and the massively parallel nature of optical systems can provide for high throughput information storage.

Photonics Center scientists and engineers are working to replace current optical storage technology with parallel channel read/write heads and photochromic optical media. This photochromic optical memory system, co-invented by Rome Laboratory and Syracuse University, is based on transition metal oxide thin films. These films change color and electrical resistance when written by light of the proper wavelengths and beam size.
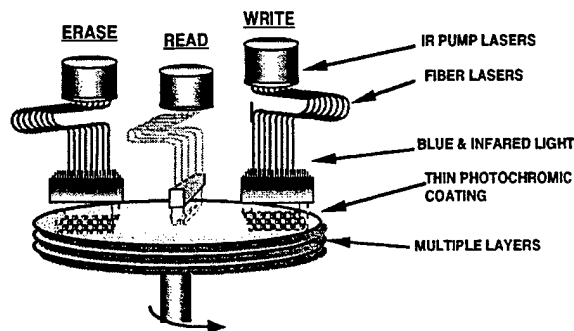
Figure 1. System Schematic.

Data stored on these optical disks can be read using changes in reflectance, electrical resistance or Raman scattering. Written spots are permanent until erased with infrared light that is powerful enough to heat the spot to over 400° C. The disk can be written using blue or ultraviolet fiber laser bundles or laser arrays allowing an entire sector to be written or read at once. Data from many sources can be simultaneously written and needed data can be read by a separate parallel channel read head.

Our current system has a better signal to noise ratio, faster access time, lower power consumption and improved data density compared to magneto-optic (MO) or phase change systems with single read/write heads. The current technology leader is phase change, which has problem of "bit creep" limiting density. MO is capable of higher density, but is expensive due to low manufacturing yields and has adhesion problems (drop outs). All removable high density magnetic systems require lasers for tracking, necessitating a dual magnetic and optical system.

The parallel nature of our system can solve the current bottleneck in transferring data from processors to memory. This bottleneck is being experienced by Air Force systems that manage massive amounts of information from multiple sources. The Air Force deficiency we are initially addressing is parallel storage and read out of events during exercises for Air Combat Command (ACC). The new memory system will also correct deficiencies identified in the Air Force Mission Support System (AFMSS), the Airborne Warning and Control System (AWACS), the Distributed Air Operations Center (DAOC) and the Joint STARS System. Civilian multimedia technology will be improved by efficiently synchronizing video and audio output while the computer is simultaneously processing user input.

This thin film memory was the result of a joint Syracuse University-Rome Laboratory effort that resulted in a patent application. The

key to our patent was our discovery that 532 nm and 1060 nm light, when spatially overlapped on tungsten oxide powder, would cause a permanent yellow WO_3 to blue W_2O_5 color change in ambient atmospheric conditions. We deduced that the 1060 nm light was heating the lattice, and allowing the material to restructure into the W_2O_5 blue form before it cooled. We reasoned that by using the 1060 nm light alone, we would be able to erase the material. We tested our theory, and the material erased completely. We also determined that heating the material above about 400 ° C for a few seconds in an oven would perform a global erase.

Our initial discovery of the effect was on loose powder, so our first priority was on producing usable forms of the material, capable of reproducible results and fixed micron size sites for repeatability and extended time studies. We have developed two forms of the material. The first we call Woxyfoil™, which consists of tungsten foil carefully oxidized on the surface only. The other is thin films of tungsten oxide deposited on quartz substrates.

1.2 Previous Experiments

Oxides in general have plenty of defects. The wide range of power indices at different incident power ranges in these experiments show the complicated nature of oxides. In WO_3, there are plenty of defect states available to undergo transitions at 532 nm. We learned that there may be no lower power limit for the read beam, if the read beam is 532 nm. So using a different wavelength further away from the bandgap of WO_3, which is about 350 to 385 nm, may be more efficient.

We used the Raman spectroscopy setup in laboratory 21 to characterize these materials as we developed them. We rebuilt our system to include more precise spot size measurement capability and to shorten the optical path lengths in the system to keep the beams as small and free of aberrations as possible. The results of our previous effort[1] showed that the 1.06 μm is acting mostly as heat, not as a transition source. Oxygen exchange with the atmosphere must be taken into account. As the medium heats up, adsorbed gases, including oxygen, desorb from the surface. This changes the rate at which oxygen can leave the lattice itself, thus changing the rate at which octahedra reform to share edges.

The Arrhenius rate law says that the reaction rate of a thermally activated process increases exponentially as the inverse of the absolute temperature increases linearly. We found that an Arrhenius type plot of the results of ramping up the 1.06 μm was not strictly linear. This indicates that the optical process is not straightforward random heating. We know that different forms of the material are absorptive at near and far IR wavelengths. We also used high peak power modelocked and Q-switched pulse trains. The combination of these two factors may have led to a nonlinear transformation and absorption process.

We found enough linear variation in response to work the system at the power density level for 532 nm light of 650 μW/μm², and for 1.06 μm light of 520 μW/μm².

We measured the noise in our Raman read process. The worst case showed a 19% standard deviation. This is still a much better raw read process, due to the zero signal on a written area, than any current optical recording system.

We also found that the distribution of Raman scattering centers, i.e. corner-sharing octahedra, on the surface of common WO_3 is spatially uniform. The density of defects, i.e. edge-sharing, oxygen deficient octahedra, scales as the square of the lateral extent of the observed region as does the topographical surface area. At the power densities employed

and the amount of oxygen substoichiometry employed, there appears to be little cooperativity between the chemistry occurring at different defect centers.

1.3 These Experiments

The excitation spectra and direct sequence of transition measurements planned for the previous effort were not performed as the system was down for six months due to laser modelocker and Q-switch failure followed by OMA detector failure.

We suggested these additional tasks at the end of the previous effort:

1.) Spatially displacing the two wavelengths to help determine the thermal transfer properties of the photochromic material.

2.) Use a tunable dye laser system to measure the excitation spectrum of the material, to tell us where the Raman signal from the material is most enhanced by resonance or by available defect or other states in the material.

3.) Use a third color displaced temporally after the blue-green and IR together. The change in reflectance and/or transmission of the third color pulse as it is stepped away from the write pulses in time, would give us information about the timing and sequencing of the light absorption, electron transitions, lattice restructuring and intervalence transfer occurring in the material.

4.) We also suggested testing whether the power levels needed to write the material were lower in the UV. The bandgap of the material is at about 350 to 385 nm, so working in the UV should give us many more transition states, which should lead to lower power requirements for writing.

The plan for this effort included performing optical power threshold experiments to determine how much light is

needed to effect the yellow to blue transition. These were performed using a visible CW laser and shutters, and later, a pulsed UV system. We had already determined that we would be able to make both forms of material we have developed so far undergo transition by either the blue-green wavelength or the IR wavelength alone.

Also, in this project, we wanted to measure the temporal pulse response, wavelength dependency and readout intensity of our new optical memory. These gave a detailed view of energy and mass transfer rates in the material. Heating, transition and cooling occur too quickly to measure by ordinary chemical means. We used these measurements to model the interaction between the two wavelengths and proved that the fixing of the material color change is due to the heating effect of the infrared wavelength.

We used a tunable optical parametric oscillator (OPO) laser system to measure the excitation spectrum of the material across the visible spectrum. This told us where the efficiency of the writing process was most enhanced by available defect states in the material.

1.4 Payoff

The Air Force requirement for dense storage memory systems will be met as quickly as possible by an early exploitation of the new discovery for disk memory systems. Successful completion of this and following efforts will lead to faster, more stable, erasable, ultra-dense optical memory systems for DoD mission planners, pilots needing mission maps and threat databases, intelligence data storage, and for command and control, radar data manipulation and battlefield management. In the civilian world, data storage is a very large multibillion dollar market. If we can begin strong commercial

licensing and development, the timeline could be 2-3 years for a civilian system (medical storage would be a good initial market), and 3-4 years for an Air Force system.

Follow on systems may include multiple layer systems, consisting of other transition metal oxides in separate layers, and an ultradense single layer system that is currently in the patent disclosure stage. According to Dr. Mansuripur of the University of Arizona, author of "The Physical Principles of Magneto-Optical Recording", we are the only viable candidate for more than two layers of memory, because we have the ability to make each individual layer spectrally selective in its absorption. This we can do by individually doping each layer for absorption of a specific wavelength.

Because these materials change electrical resistance when they change colors, they can be used to make an optically addressable electronic memory capable of reading an entire page of optical data from a 3D optical memory or an entire optical memory card. The Air Force can use this initially in compact medical and maintenance records storage.

2   Theory

2.1   Background

Simultaneously presented YAG laser beams at 1.06 microns and (doubled YAG) at 532 nanometers can be used to write bits on films. The 532 nanometer radiation causes a fast electron transfer which is manifested in a yellow to blue color shift. The shift is made permanent by the heating effect of the 1.06 micron beam (milliseconds) which drives out weakly bonded oxygen. This is the chemical reaction

$$4WO_{3(s)} \underset{400K}{\overset{h\nu}{\rightleftarrows}} 2WO_5 + O_{2(g)} \qquad (1)$$
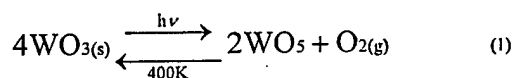
which is permanent until the material is reheated to a temperature greater than 400° C. Bits are read in less than 2 nanoseconds using the direct reflection or the Raman emission of the 532 nanometer laser used alone. Erase is accomplished using the 1.06 μm beam alone.

2.2   Structure of WO_3 and M_xWO_3

WO_3 has a distorted version of the ReO_3 structure (Figure 2a), which is a simple cubic lattice of tungsten with each tungsten atom the center of a WO_6 octahedron. Figure 3 shows a more accurate representation of the WO_3 structure.
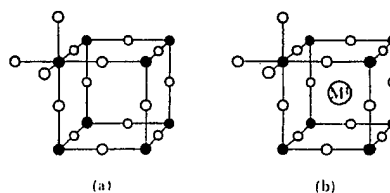

Figure 2. Filled circles are W^{6+}, open circles are O^{2-}, M^I is a metal ion[2].
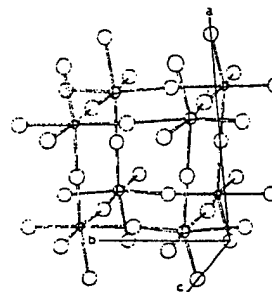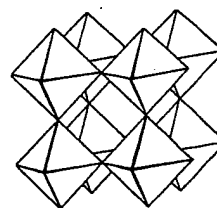

Figure 3. WO^3 structure[3].

Figure 4. MO^6 octahedra stacking[4].

When small amounts of metals (M), usually protons from hydrogen or sodium metal, are added to WO_3, a tungsten bronze, M_xWO_3, is formed. The WO_3 lattice

restructures with a proton or a positive metal ion in the center of the simple cubic tungsten lattice (Figure 2b), and the material turns blue. In tungsten bronzes, metal atoms donate their electrons to the empty conduction band of the host WO_3 lattice. These extra electrons lead to a semiconducting or a metallic state, depending on x. The octohedra stacking is shown in Figure 4. Notice that in WO_3, the octahedra share corners only.

2.3 Shear Planes in Substoichiometric WO_3

When WO_3 is heated in vacuum, oxygen and water are driven off, and the material becomes substoichiometric WO_{3-x} with x being a small number.
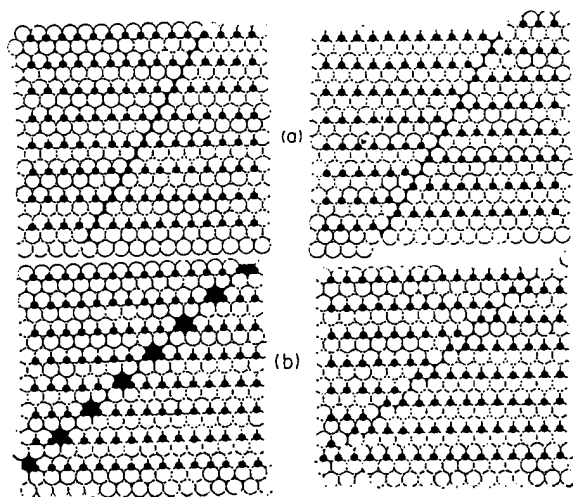

Figure 5. Antiphase boundary (on left) and crystallographic shear (on right) along 2 different crystallographic directions[5].

As illustrated in Figure 5, when the material is being heated, oxygen vacancies preferentially form discs and then planes. These planes are called antiphase boundaries. When there is enough energy in the lattice, the lattice shears along the plane of vacancies, removing the vacancies. This is called crystallographic shear. In WO_3, the WO_6 octahedra share corners before shearing, as is

shown in Figure 4. After shearing, some or all neighboring octahedra along the CS plane share edges, as shown in Figure 6. This results in removing some oxygen atoms.

c
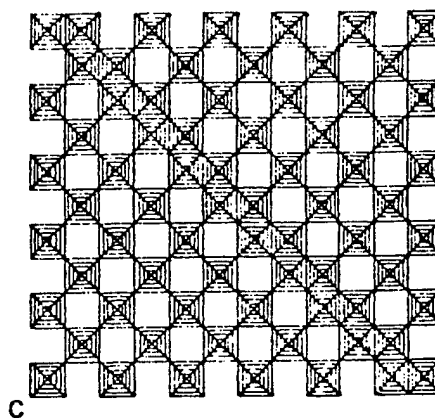
Figure 6. A {001} shear plane in WO_3. Shaded areas are WO_6 octahedra as viewed from above[6].

Crystallographic Shear (CS) or Magnelli phases are quasistable. In WO_3 they initially are of the form M_nO_{3n-1}, and occur along the {102} crystallographic direction. These range from $W_{25}O_{74}$ ($WO_{2.96}$) to $W_{15}O_{44}$ ($WO_{2.933}$). Further reduction causes the CS planes to occur along the {103} crystallographic direction, and create phases of the form M_nO_{3n-2}. These include $W_{50}O_{148}$ ($WO_{2.96}$), $W_{40}O_{118}$ ($WO_{2.95}$) and $W_{20}O_{58}$ ($WO_{2.90}$). In addition, {001} shear planes have been reported[6].

Figure 7. Idealized structure of W_2O_5 ($WO_{2.5}$)[7].

The theoretical form of W_2O_5 ($WO_{2.5}$) is shown in Figure 7. There is also a unique extremely stable phase that forms readily under a wide range of conditions when WO_3 is reduced. This is $W_{18}O_{49}$ ($WO_{2.72}$), as shown in Figure 8.

5

(b)

Figure 8. $W_{18}O_{49}$ ($WO_{2.72}$)[8].

MO diagram for WO_6 Density of States for WO_3
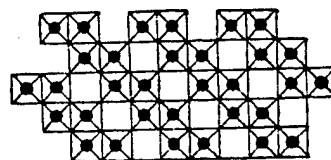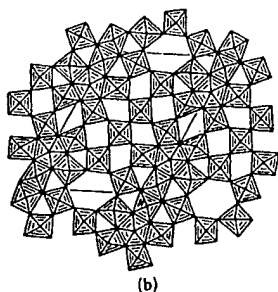
2.4 The Band Structure

In WO_3, the Mg^+/Mg^{2+} of Figure 9 is replaced mostly by $W^{6+}(5d)$ orbitals. The Madelung potential is an electrostatic potential acting on an electron due to the ionicity of the lattice. The polarization is the polarization the electron causes in the nearby lattice. The overlap is the broadening of electronic levels due to the spatial overlap between ions.
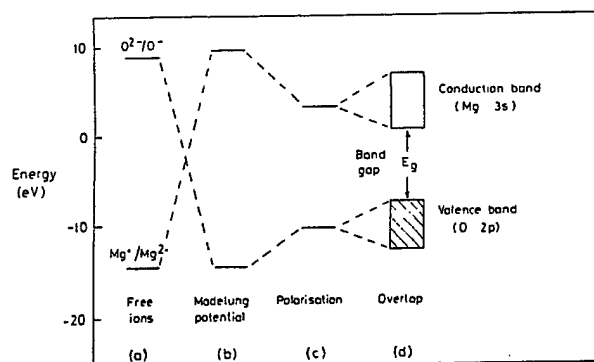
Figure 9. Ionic-model of the band gap in MgO[9].

WO_3 is more complex than the simple picture of Figure 9 for MgO. In WO_3, since the $O^{2-}(2p)$ orbitals are lower in energy than the $W^{6+}(5d)$ orbitals, the empty valence band is formed from a bonding combination of the $O^{2-}(2p)$ orbitals and mostly the $W^{6+}(5d)$ orbital. Similarly, the conduction band is formed from an antibonding combination of the $O^{2-}(2p)$ orbitals and mostly the $W^{6+}(5d)$ orbital.
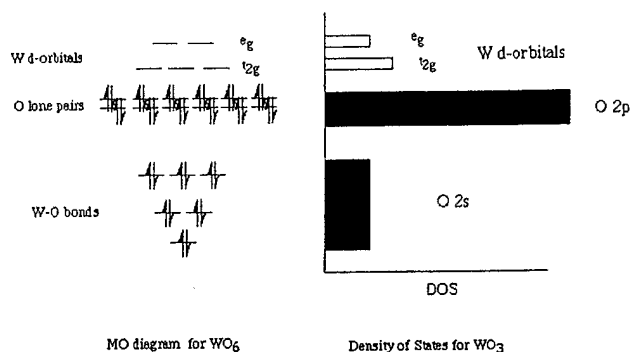
The band gap, E_g, is about 2.7 eV for WO_3. This is a small energy compared to the much larger effects shown in Figure 9. The band gap can not yet be accurately calculated from the spectroscopic levels, then applying the Madelung potential and so on. It must be measured, as it was for Figure 11, which shows the allowed transition of electrons from the top of the filled band to the bottom of the empty band.
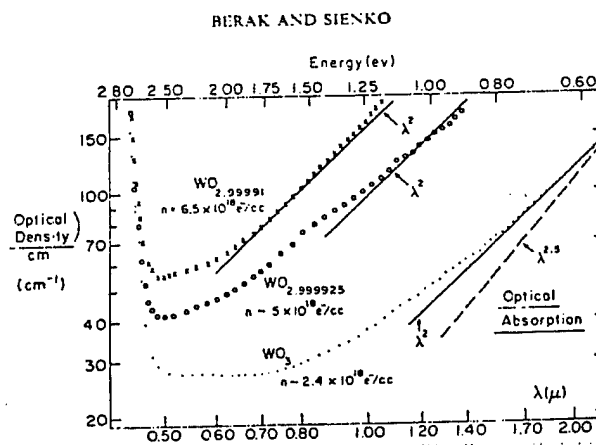
Figure 11. Optical absorption vs. wavelength for 3 crystals varying in W/O ratio[11].

Although WO_3 has a small semiconductor-like band gap, many other transition metal oxides end up with a wider gap, and thus are insulators, or have overlap between the valence and conduction bands, and thus are metallic.

3 Experimental

3.1 488 nm with 1.06 μm Threshold and Time Delay Measurements

3.1.1 Introduction

In our last AFOSR sponsored effort[1], we came to the conclusion that the IR light acted almost entirely as heat on the material, not as a transition source. We ramped the IR power while keeping the green 532 nm light constant, and found that the decay in the Raman counts as the 1.06 μm was increased was exponential. The Arrhenius rate law says that the reaction rate of a thermally activated process increases exponentially as the inverse of the absolute temperature increases linearly.

We also found that we could completely change over the material ramping 532 nm only, but adding a small constant amount of 1.06 μm at the same time prevented complete turnover. This led us to believe the 1.06 μm was acting to keep the lattice soft and prevented it from restructuring into the W_2O_5 form. We determined the temperature of the material by measuring the linewidth broadening of the Raman peaks and comparing their linewidth to peaks taken at measured material temperatures. This showed that the temperature rise with increased incident power was less than linear, and we hypothesized that the O_2 leaving the material carried some of the heat away with it.

In this effort, we tried to further separate the effects of the two wavelengths by preheating the material with IR before the transition source lower wavelength light. We did this in order to get information about the timing and sequencing of the light absorption, electron transitions, lattice restructuring and intervalence transfer occurring in the material.

For this effort, we used 488 nm and 1.06 μm light. Because we had performed threshold measurements with 532 nm and 1.06 μm before[1], we wanted to determine the threshold for write using 488 nm and 1.06 μm and see if using transition light closer to the bandgap of tungsten oxide made any difference.

3.1.2 Experimental

1.06 μm CW from a Quantronix Model 4116 Nd:YAG laser was amplitude controlled using a circular variable OD filter. The CW 488 nm light from a Spectra-Physics Model 2060-10S was amplitude controlled by a CRI Model LPC-VIS laser power controller (LPC). Each wavelength was individually shuttered using a Vincent UniBlitz Model UHS1T2 Shutter driven by a Vincent UniBlitz Model T132 Shutter Driver. Both wavelengths were added collinearly through a 1.06 μm reflective mirror. The beam then was sent through a 5x or 10x microscope objective. The small spot was incident normally to the sample, and some of the reflected light as well as some of the Raman scattered light were directed to the optical multichannel analyzer (OMA). All measurements in this section were on oxidized tungsten foils ("woxyfoils"). Some light was split off using a beamsplitter into a Pulnix Model TM-540 CCD camera.
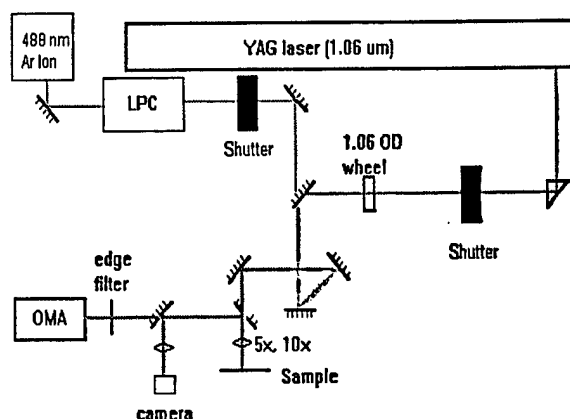

Figure 12. Experimental Setup.

The OMA gives a plot of counts vs. channel number, or when calibrated, counts vs. wavelength. Figure 13 shows a typical result. The highlighted area in the largest peak is the integration interval whose integrated total counts are saved as the data for each exposure. These totals are then plotted as individual data points in a single graph after all the exposures are completed, as shown in Figure 14 and following plots.

The OMA does not start counting photons immediately. There is a 16 ms dead time at the beginning of the OMA accumulation. As there is more power to convert WO_3 to W_2O_5, more material is being converted in the dead time, and the total count rate decreases.

had a pulse energy of 6.94 mJ/pulse. The spot size (diameter) was[1] 1.4 μm, so using area = πr^2 = 1.54 μm^2, the energy density was 4.51 mJ/μm^2.
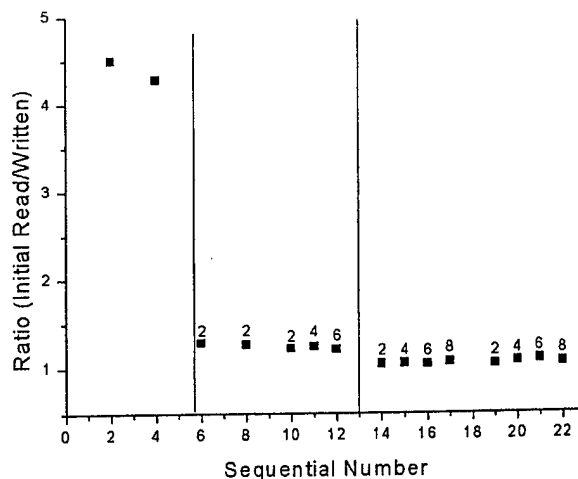
Figure 14. IR ramp threshold measurement.

We varied the pulse energy of the 1.06 μm pulses. The sequential number (the X-axis) is the number of the spot on the material surface. The number above the data point is the number of pulses per spot.

The initial average power for the 1.06 μm pulse train was 1.39 μW. The 1.06 μm pulses were also 2 ms in duration and occurred every 400 ms. The 1.06 μm pulse energy for sequential numbers 2 and 4 was 0.552 μJ. There were 2 pulses on each spot. Since the ratio was much greater than one, the material was written on these spots.

We decreased the 1.06 μm pulse energy for sequential number 6 through 12 to 0.276 μJ, and the pulse duration for the IR pulse was changed to 1 ms per pulse. Although some spots have ratios slightly greater than 1, and even though we attempted up to six pulses per spot, we did not strongly write the material, due to the low strength of the IR light.

We increased the 1.06 μm pulse energy for sequential number 14 through 22 to 0.444 μJ and increased the IR pulse duration to 2 ms per pulse. Even though we attempted up to
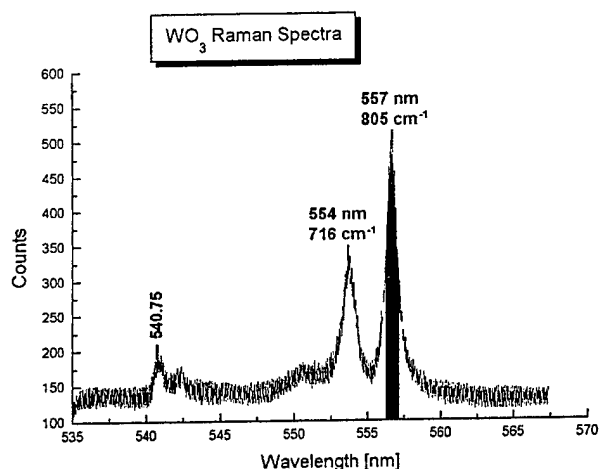

Figure 13. Typical Raman Spectrum

3.1.3 Threshold Results & Discussion

Figure 14 shows the ratio of the reflectance of the initial unwritten spot to the reflectance of the written spot. The read and the write used the 488 nm light. The read occurred during the write. The visible (488 nm) and IR (1.06 μm) pulses were coincident both in time and in position on the surface. They were 2 ms in duration and occurred every 400 ms. The average power for the 488 nm light was 17.35 mW. The 488 nm pulses

8

eight pulses per spot, we again did not strongly write the material.

Thus, for power regulated 2 ms duration 488 nm pulses with an energy density of 4.51 mJ/μm^2, the energy threshold for 1.06 μm is between 0.444 μJ and 0.552 μJ. Since the spot size was determined[1] to be 1.4 μm, and using area = πr^2 = 1.54 μm^2, the energy density threshold is between 0.288 μJ/μm^2 and 0.358 μJ/μm^2.

In order to determine the effect of pulse duration on the contrast ratio, we increased the pulse duration of both wavelengths to 10 ms, so then the 488 nm pulses had a pulse energy of 34.7 mJ/pulse. The 10 ms pulses were still coincident every 400 ms. The 1.06 μm (Nd:YAG) pulse energy varied. Once again, all reads were during writes. Only one pulse was incident per spot. Figure 15 shows the result.

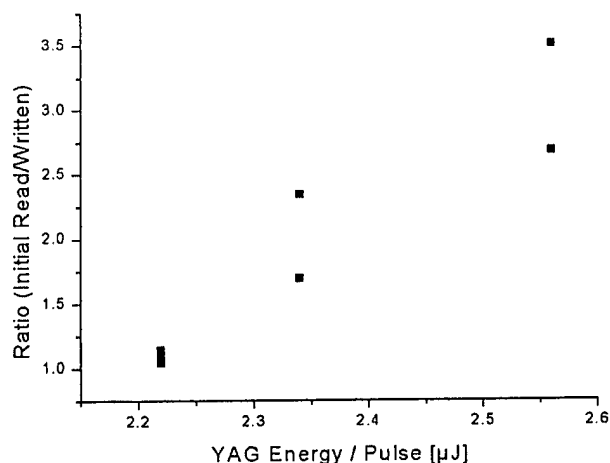Was smaller than the 4.5 achieved with two successive 2 ms pulses in Figure 14.

Figure 16 shows an IR ramp measurement with the 488 nm pulse energy reduced to 27.2 mJ. Once again, all reads were during writes and used the 488 nm light. Only one pulse was incident per spot. The IR power was varied by changing neutral density (ND) filters in the IR beam. Two things should be noted in comparison to Figure 15, where the 488 nm pulses had pulse energy of 34.7 mJ. One is that the threshold for writing is between the same two sets of YAG pulse energy data points, and the other is that the set of data points in Figure 16 at around 2.57 μJ/pulse show a decrease in writing efficiency. In Figure 16, the erasing (blue back to yellow) effect of the 1.06 μm light overcomes the writing (yellow to blue) effect of the 488 nm light.

Figure 15. IR ramp measurement.
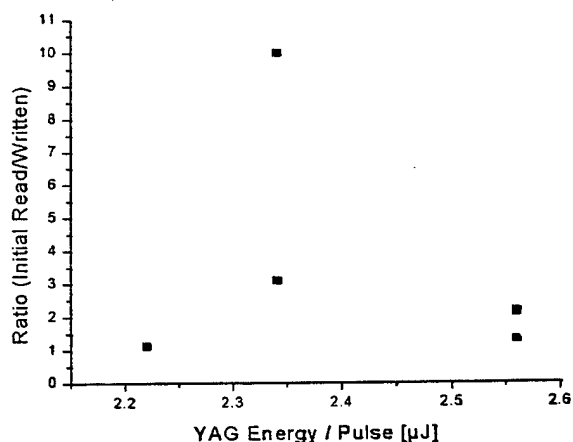
Figure 16. IR ramp measurement.

In this case the threshold was between 2.22 μJ and 2.34 μJ for each 10 ms pulse. In Figure 14 the threshold for 2 ms pulses was between 0.444 μJ and 0.552 μJ. Multiplying the 2 ms thresholds by 5 (10ms/2ms = 5) gives 2.22 μJ to 2.76 μJ. These numbers are comparable to the actual 10 ms numbers, showing that the increase in time had little effect on the threshold, but the contrast ratio

Comparison of these 488 nm and 1.06 μm results with 532 nm and 1.06 μm results from the previous effort[1] is difficult. In the previous effort, we got a 2:1 ratio with 120 mW average power of 532 nm from a frequency doubled mode-locked Q-switched Nd:YAG laser. We used 8 mW average power of 1.06 μm from the undoubled mode-locked Q-switched Nd:YAG laser. The spot size was approximately 7 μm. The corresponding

average power densities were around 3.1 mW/μm^2 for the 532 nm beam and 208 μW/μm^2 for the 1.06 μm light. The duty cycle of the laser was 9×10^{-6}, so the peak power densities were about 344 W/μm^2 of 532 nm light and 23.1 W/μm^2 of 1.06 μm light. Because of the high peak power and low duty cycle, these results can not be directly compared to CW modulated 488 nm experiments. Instead, we should frequency double the Nd:YAG in CW mode. We should be able to get a few mW of CW 532 nm to use. This may require either two Nd:YAG lasers or removing the internal mode control aperture of a single one to let it mode hop and get increased CW power, as the doubling efficiency of CW light is very poor.

For the data in Figures 14 to 16 the read of the written spot was during the write. We wanted to see how the ratio changed after the write. Figure 17 shows the results.
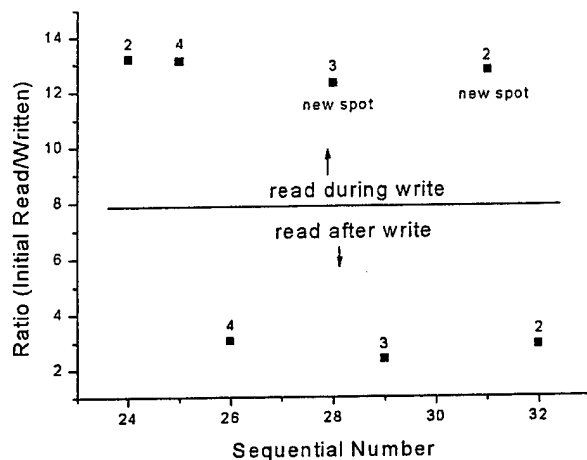

Figure 17. Ratio during and after write.

The difference was that in the read during write, the 1.06 μm is on the spot, and is acting to keep the octahedra from forming in either the WO$_3$ or the W$_2$O$_5$ state, but in the read after write, only the 488 nm is present. Note that the "after write" ratios are about 2 to 3, which is still excellent compared to other optical memory media.

For this experiment we used 10 ms coincident pulses every 400 ms. The pulse energies were 34.7 mJ for 488 nm and 2.76 μJ for 1.06 μm. The number above the data point is the number of pulses per spot. The larger "during write" ratio compared to Figure 15 can only be due to the increased number of pulses per spot, since these experiments were performed on the same material on the same day with identical 488 nm pulse energy.

3.1.4 Time Delay Results & Discussion

Figure 18 shows 20 ms blue (488 nm) pulses delayed 20 ms after 20 ms IR (1.06 μm) pulses. In this section, the 488 nm beam was kept at a constant CW power of 247 μW, and the IR CW power was something less than 10.75 mW.

Notice that the read during write and after write numbers are about the same. Because of the delay between the two wavelengths, the 1.06 um is not on the spot when it is read in both cases.
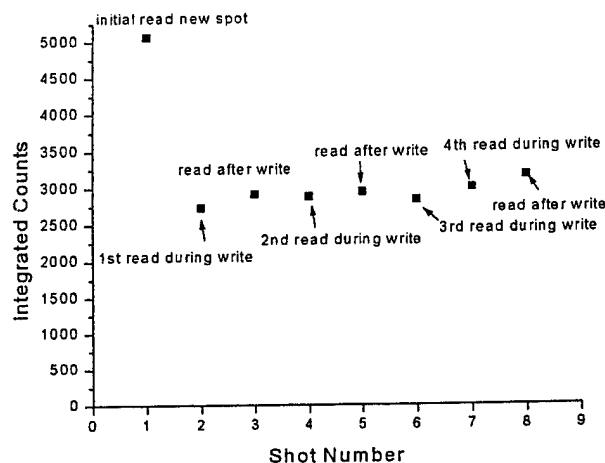

Figure 18. IR preheat.

To compare to previous figures, the ratio for Figure 18 would be Initial Read counts/Written counts or 5000/2500 = 2. Since these pulses are "back to back", and the results are about the same as in Figure 17, the lattice reconfiguration time into the final state must

10

be less than a ms or so using these wavelengths.

In order to make sure that the results were not due to a difference in power levels on different days, we repeated the 20 ms blue coincident with 20 ms IR (Figure 19), and got the same results as Figure 17 for this case. For Figure 19, the ratio was Initial Read counts/Written counts or 5000/2000 = 2.5 for read after write.
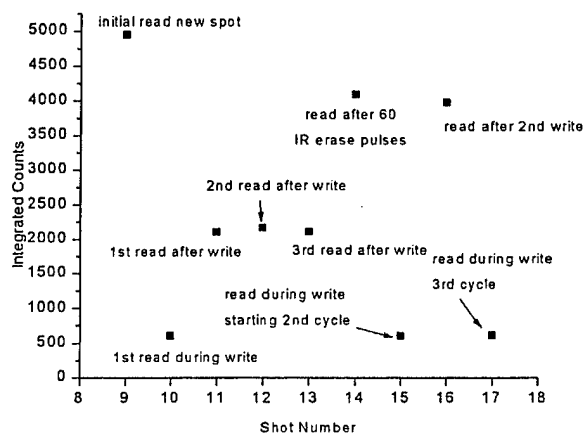

Figure 19. Coincident pulses.

Notice that the erased spot has lower counts initially, but returns almost to its erased level after the second write. Since these were single shot measurements, this may be an artifact related to the 16 ms dead time of the OMA, and should be explored further.

Figure 20 shows 235 μW blue 20 ms pulses that were delayed compared to the 12 mW IR 20 ms pulses. These high power levels were selected as being closer to the mode locked Q-switched 532 nm power levels of the previous effort[1]. The read occurred during the write and used the 488 nm light. Because the ratios from 10 to 20 ms delay shows somewhat ambiguous results, we hypothesized that the 16 ms delay time of the OMA might contribute to these results. The accumulation time of the OMA during these experiments was 2 seconds, so the fact that the break occurs near the 16 ms dead time of the OMA is coincidental.
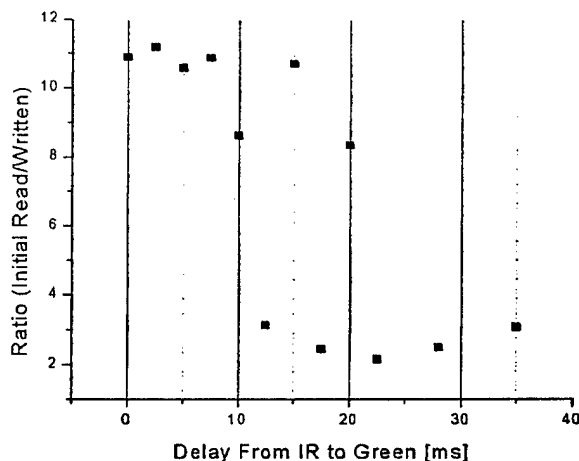
Figure 20. Variable delay.

3.1.5 Conclusions

These measurements showed that writing the material was possible by preheating the material with IR. So the two wavelength beams will not have to be strictly coaxial when writing the material, relaxing the requirements for a write head in a disk drive.

This effort and the preceding effort have conclusively proven the 1.06 μm light acts only as heat.

3.2 Ultraviolet measurements

3.2.1 Introduction

The switching and memory efforts at the photonics center have primarily used 488, 532, 985, 1060 nm wavelengths. We wanted to see if the power levels needed to write the material decrease as we got closer to the bandgap. It has been well known that the efficiency of the material increases with shorter wavelengths, but these sources are difficult to obtain. The bandgap of the material is at about 350 to 385 nm, so working in the UV should give us many more transition states, which should lead to lower power requirements for writing. More states should

also lead to faster color change. Yoshiike[12] demonstrated a 200 ps color change at 337 nm. This chapter describes the effort of obtaining material thresholds at 385 nm.

3.2.2 Experimental

Figure 21 shows the setup we used to perform threshold measurements at 385 nm on sputtered[13] thin films. The 385 nm laser system was custom built for us by Gary Vaillancourt of L&E Associates. A Nd:YLF laser rod was used and output 1047 nm light. The rod was positioned in the laser cavity between two curved mirrors. The beam waist was at the output mirror. Before the output mirror, the beam passed through a frequency doubling crystal which allowed light at approximately 523-527 nm to pass through. The green beam was incident on a turning mirror which sent the light into a second laser cavity. The beam passed through the back side of a curved mirror and through a Ti:Saphire crystal. The green beam acted as a pump for this crystal which lased at 780-790 nm due to the curved mirrors. The red light was frequency doubled which gave blue light at approximately 385-395 nm. All three colors, green, red, and blue passed through the output mirror and a dispersion prism where the colors became physically separated. The green and red beams were blocked and the blue light continued in the optical train. The blue light was pulsed at approximately 1kHz with 100 ns pulse width. The blue beam was

incident on a turning mirror and it then passed through a rotating graded neutral density (ND) filter. The beam passed through two pellicles, then a 20X Olympus objective with a numerical aperture (NA) of .4 and was finally incident on the thin film. The second pellicle reflected approximately 8% of the blue light which was detected by a Newport power meter model # 1830C. This was to allow calculation of the incident power level of light on the
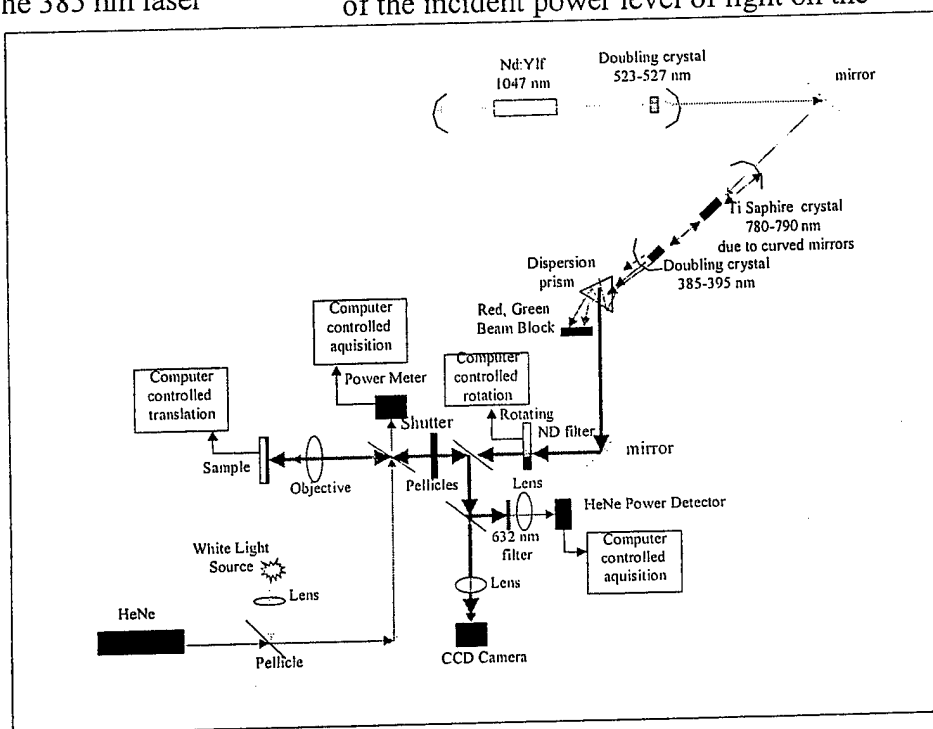
Figure 21. Schematic of system for UV power threshold measurements

film. Also incident on the film were a HeNe beam from a Hughes Aircraft Company laser, model # 3225H-PC, and white light coming from a separate optical train. White light was introduced and was collinear with the HeNe path by using a 40% reflective / 40% transmitive pellicle. The white light provided illumination of the sample to allow visual inspection of written spots through the use of a Pulnix model TM-540 CCD camera that was connected to a monitor. All three sources were reflected off the film and directed down a different path. The camera saw the film through the white light and a UDT model

5390 Optometer with a Si detector head model 247 measured the reflectance change of the HeNe beam on the film by measuring the power before a spot was written and after a spot was written. The system was completely automated by a Labview program which is documented in Appendix A. Three trials were taken at each ND position on the wheel and then the values were averaged to generate some plots. The filter rotated 2 degrees for each trial and was controlled by a Klinger rotation stage. The film was mounted on an automated Klinger xyz translation stage. Three fresh film areas were used for each power position. Individual UV pulses were incident on the film for each trial.

3.2.3 Results & Discussion

Figure 22 shows the power dependence of the ND filter wheel based on its position. This was obtained by putting a power meter in the position where the film was normally located.

Each data point represents the average of 6 trials for each wheel position. There was a

large variation most probably due to the fact that the power meter was slow compared to the duration of the pulse therefore leading to a large variation. The tendency was correct in that it decreases with wheel position because it was becoming a stronger ND filter as it rotated.
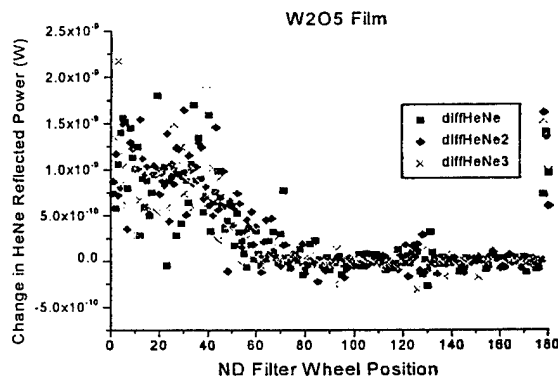

Figure 23. W_2O_5 on quartz. Threshold is approximately at wheel position 80.

An exponential decay fit was performed to give the general pattern. Perhaps a more accurate fit can be performed, but the values given for the fit are a close representation of the average power incident for that specific wheel position. This graph can be used as a reference to determine the approximate power level of a particular wheel position for graphs that follow.

The threshold for Figure 23, which shows W_2O_5 alone on quartz, is about 30 µW. This power value was determined from Figure 22. Since the repetition rate was 1 kHz, the pulse energy was 30 x 10^{-6} W/(1000 pulses/s) = (3 x 10^{-5} J/s)/(1 x 10^3 pulses/s) = 3 x 10^{-8} J/pulse = 30 nJ/pulse. The spot size was
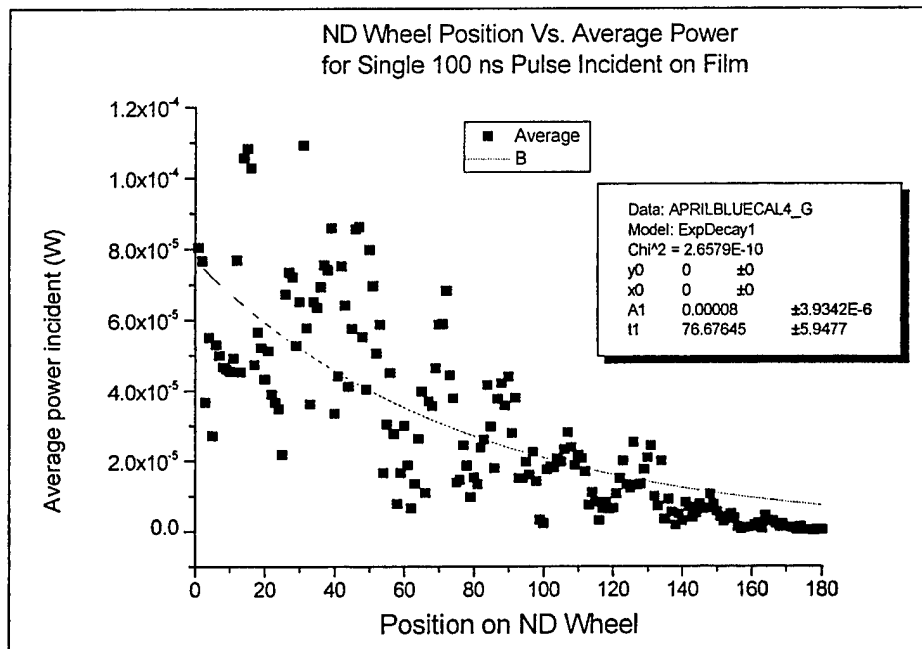

Figure 22. ND wheel position vs. average power for single 100 ns pulses that would be incident on the film.

13

1.17 μm, so using area = πr^2 = 1.08 μm^2, the pulse energy density was 27.9 nJ/μm^2 for these 100 ns duration 385 nm pulses. In Section 3.1.3, we noted that the pulse energy density threshold for 2 ms duration 488 nm pulses used in conjunction with 2 ms duration 1.06 μm pulses and a 1.4 μm spot size was 4.51 mJ/μm^2. Because of the difference between gated CW 488 nm and high peak power 385 nm UV pulses, no direct comparison can be made in this case, but we can compare to the 532 nm mode-locked Q-switched results from the previous effort[1].

The 385 nm pulse width was 100 ns. The peak power was then 0.3 W. Using the area of 1.08 μm^2, the peak power density for 385 nm pulses was 0.278 W/μm^2. The 532 nm mode-locked Q-switched thresholds were at peak power densities of about 344 W/μm^2 of 532 nm light and 23.1 W/μm^2 of 1.06 μm light. The difference is a factor of 1000 for different electronic excitation wavelengths, but the 385 nm had no IR light present to separately heat the surface.

Disks spinning at the speeds used in commercial systems require about 50 ns write speeds, so these measurements are very close to valid system requirement numbers.
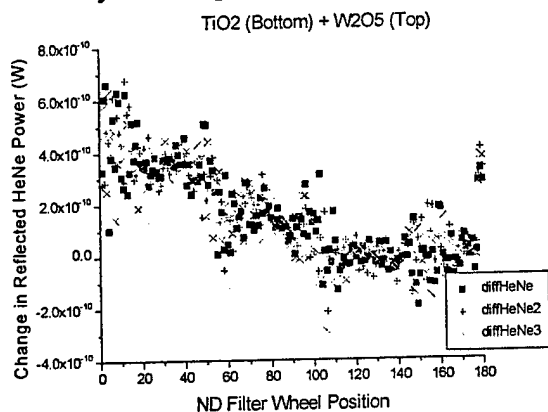

TiO2 (Bottom) + W2O5 (Top)

Figure 24. W$_2$O$_5$ on TiO$_2$ on quartz. Threshold is approximately at wheel position 100.

It is also exciting to see that adding a layer of titanium oxide whether below or above the W$_2$O$_5$ layer lowers the power

threshold compared to writing on W$_2$O$_5$ alone. Adding TiO$_2$, as shown in Figures 24 and 25, lowers the threshold from 30 μW to approximately 20 μW.
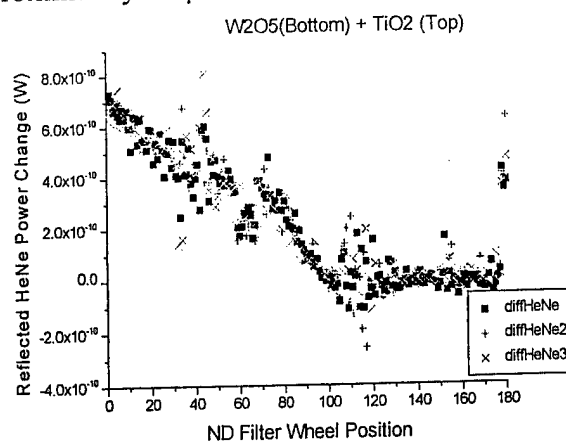

W2O5(Bottom) + TiO2 (Top)

Figure 25. TiO$_2$ on W$_2$O$_5$ on quartz. Threshold is approximately at wheel position 100.

A solution of silver colloid was prepared and a droplet of the mixture was placed on each of the previous samples. This was done to test if the silver particles aided in lowering the threshold of writing power. However, the solution turned the films from appearing blue in color to clear or yellowish. We were not able to write on this area with our apparatus.

Bianchin[14] showed that doping amorphous tungsten oxide in the proper manner can aid in electrochromism. He also explains that silver in particular actually acts as an inhibitor for the reversibility of electrochromism which explains why trying to write on film areas where the droplets of silver colloid were applied did not work. He further explains that a dopant such as hydrogen endows electrochromic materials with remarkable properties.

We were able to access some proprietary sol-gel process tungsten oxide films. We electrochemically reduced some of them and tested them.

Figure 26. Written spots on a proprietary sol-gel process film. Spots are 15 microns apart. The large white spot in the top center is the HeNe beam being reflected into the camera

We were successful at writing on all of these films. Power thresholding tests were not performed as in the above graphs, but Figure 26 depicts written spots on these films.

3.2.4 Conclusions

At the time the 385 nm experiments were performed, writing at 100 ns was the fastest speed achieved. To use this material in the commercial memory world, write speeds need to occur in the 50 ns range. So these experiments were approaching this range.

Writing on the Donnelly films proved to be exciting because they were made from a completely different process. Using their form of fabrication could reduce manufacturing costs if this material entered the memory commercial world.

Tungsten oxide based media compare well with existing optical data storage media in all performance categories tested to date. Write power threshold and write speed are quite appropriate for a variety of data storage applications. The contrast between written and unwritten spots for tungsten oxide based media far exceeds those of the other media. Intracavity doubling of existing small lasers may be adequate for producing disk drives.

3.3 OPO measurements

3.3.1 Introduction

Our next step was to use a tunable optical parametric oscillator (OPO) laser system to measure the excitation spectrum of the material. This told us where the efficiency of

the writing process was most enhanced by available defect states in the material.

3.3.2 Experimental

These experiments were performed in collaboration with Syracuse University to perform tests using the visible wavelength range, 400-700 nm, on thin films of tungsten oxide. Figure 27 depicts the assembled apparatus.

Pulses of continuously wavelength tunable light were obtained from a laser system which consisted of a Coherent Infinity YAG laser pumping a Coherent Model XPO optical parametric oscillator. All measurements were made with single pulses of 2.5 ns duration selected by manual shuttering of the OPO pulse train. Given that these are room temperature condensed phase samples, the fact that the spectral bandwidth of the OPO pulses varies somewhat over the tuning range is of no relevance.

The light from the OPO first traversed a non-polarizing beamsplitter, which brought half of the pulse energy to a Gentec ED-200 pyroelectric joulemeter. This joulemeter had a flat response over the entire tuning range of the OPO and so for relative measurement of action spectra, no further calibration of the detector response was required. Having this joulemeter in the apparatus allowed a relative measurement of the actual pulse energy used for each spot. The light transmitted through the beamsplitter then traversed two pellicles before being brought to a focus by a Mitutoyo

Figure 27. Schematic system used for visible wavelength range using OPO laser.

objective with an NA of 0.4 onto the sample. At 500 nm wavelength the theoretical FWHM spot size was approximately 765 nm in diameter.

After traversing the sample and the substrate, the OPO light entered another objective which recollimated it. This light was brought to a separate detector (Si photodiode) which allowed measurement of the relative amount of light penetrating the film and its substrate.

The writing efficiency is defined as the change in transmission of a 632 nm HeNe laser (Melles Griot) through the irradiated spot. For this purpose the HeNe was brought to a focus using a microscope objective onto the same spot as was irradiated by the OPO pulse. The HeNe light transmitted through the film was then recollimated by the other microscope objective with an NA of 0.25 and directed by a pellicle through a 632 nm bandpass filter onto the active region of a silicon photodiode (Newport 883-SL). To allow for constant checking of the alignment of the write (OPO) spot with the read (HeNe) spot, white light was used together

with a Pulnix CCD camera to image the region under study.

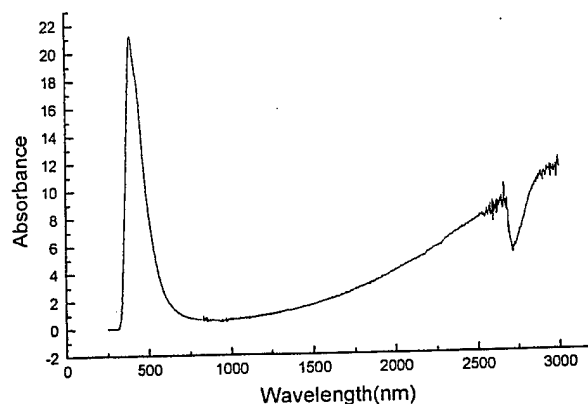### 3.3.3 Results & Discussion

Figure 28. Absorption spectrum of blue sputtered film

For the OPO experiments Figures 28 and 29 show UV-visible absorption spectra of two sputtered films selected as being typical of moderately deoxygenated (blue) and fully oxygenated (yellow) films respectively.
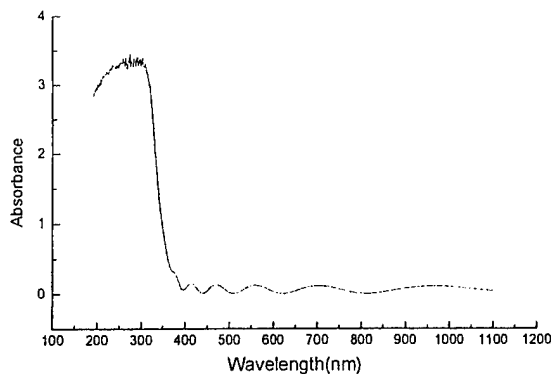
16

Figure 29. Absorption spectrum of yellow sputtered film.

The yellow film was 388 nm thick and the blue film was 488 nm thick. The interference fringes are evident for the oxygenated film. We also looked at a yellow film made by a sol-gel process.

The reason for choosing HeNe light as a monitor of spot formation is clear based on the difference in absorption of the two films at that wavelength. By using sufficiently high pulse energies, it was possible to produce spots at every wavelength from 620 nm to 410 nm, which was the limit of the OPO tuning range. As shown in figure 28 the blue films proved to be the most absorptive in the OPO tuning range and hence most photosensitive. The blue films were also thinner. It turned out that, in the case of the blue film, the spots seen on the camera were produced by ablating the tungsten oxide film completely from the substrate. This was easy to confirm beyond visible inspection using a profilometer. So only the yellow film data was used. It was not possible to obtain a precise power budget for the optical system but an upper bound for the threshold write energy at 500 nm was approximately 10^1-10^2 nJ.

Figures 30 and 31 show normalized action spectra of the oxygenated (yellow) sputtered and sol-gel films, respectively, in which the action is the change in transmitted

632 nm light. To obtain these spectra, the power of the HeNe light transmitted through a film was measured before and after exposing the film to a single pulse of the OPO. In Figures 30 and 31, the wavelength corresponding to the depressions show
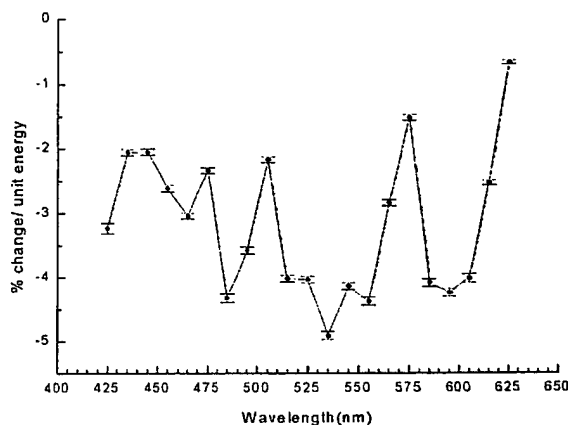

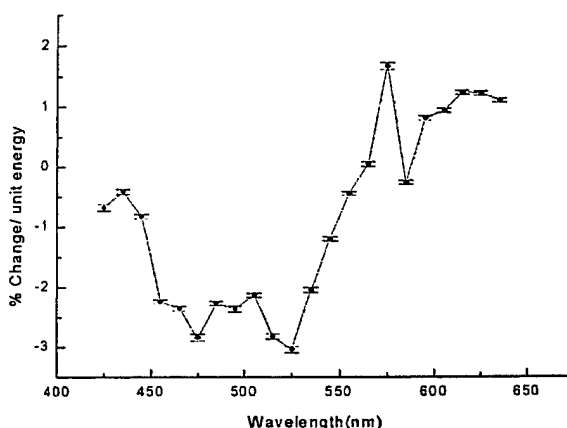**Figure 30. Action spectrum of sputtered yellow film.**

Figure 31. Action spectrum of sol-gel yellow film

where the material is most absorptive for HeNe 632 nm light. At every tested wavelength exposure, however, spots were visually written. The raw measurement at each OPO wavelength consisted of subtracting the transmitted power after the write from the transmitted HeNe power measured at the same spatial location before the write. These figures were normalized in

17

order to compare these data with each other in a way that reveals the medium's intrinsic sensitivity to the light requires some normalization.

Since the HeNe spot size was constant as the OPO wavelength was changed, and the written spot size changed with it, a normalization of the transmitted HeNe power was needed to account for the variation. Since the transmitted power scales with the area of the spot, and the area scales as the square of the diffraction limited spot size, the difference in transmitted power was scaled accordingly to account for the variation with OPO wavelength. Although the OPO power was adjusted at each wavelength to ensure that it was roughly constant with wavelength, each raw HeNe transmittance change was normalized to the actual measured OPO pulse energy for that exposure. Finally, we also normalized each raw transmittance change at each OPO wavelength to the measured absorbance of the films at the corresponding wavelength. Thus, the data displayed in Figures 30 and 31 are properly normalized for pulse to pulse OPO pulse energy variations, the change in the size of the diffraction limited spot sizes with varying OPO wavelength and the variation in absorption strength of the films with OPO wavelength. This normalized transmittance change is what appears in arbitrary units in Figures 30 and 31.

Optical Parametric Oscillator (OPO) measurements of writing efficiency vs. wavelength showed that there were two subbandgap (higher than 350 nm) wavelength ranges for each type of film that had good writing efficiency. These are probably due to defect states of the material. We want to point out that we had previously written using 488 nm and 532 nm light and observed good contrast, even though these wavelengths were outside the most efficient regions, as shown in Figures 30 and 31.

When experiments were performed on the visible wavelength dependence data, it became evident that it is possible to write in 2.5 nsec at all wavelengths used, and this shows that this medium is sufficiently fast to be amenable to any type of spinning disk format currently in use or envisioned. The raw measured difference in transmitted HeNe power represents a huge contrast between written and unwritten states compared to either PC or M-O media. PC media[15] claim a difference of about 8% reflectivity between the written and unwritten states whereas the change in optical rotation induced by M-O write[16] is about 1 part in 10^3. Thus, tungsten oxide media are clearly equal to or superior to existing media in both write speed and read contrast.

3.3.4 Conclusions

The wavelength dependent data are absolutely striking in at least two important aspects. First, for practical purposes it is clear that there is ample sensitivity at accessible wavelengths for manipulating the medium using either existing lasers or others[17] which are known to be currently in development. This would include monolithic diode pumped YAG lasers and their frequency doubled versions, both of which are now commercially available in small OEM packages, as well as GaN based devices which are in active development.

The power needed to write is small compared to that delivered in the single Q-switched pulses produced by the monolithic devices. Since these can be passively Q-switched lasers as well as CW lasers, time synchronization and data rate issues will determine what type of modulation and interconnect technology needs to be employed to produce actual commercial devices. Therefore, sufficient components exist for producing disk drives which could

utilize tungsten oxide as the recording medium.

Second, for purposes of understanding the nature of the write process in tungsten oxide based media, the presence of wavelengths where there is a marked sensitivity is obvious. Note that, as expected[18], the transmittance change is opposite in sign depending on whether the medium is initially blue or not. Given the conventional wisdom concerning the write process[19], one expects the sensitivity of either modification, i.e. fully oxygenated or oxygen deficient, to increase with decreasing wavelength until one reaches the band gap energy. Since, in these experiments, we could not reach the band gap wavelength, i.e. about 350 to 385 nm, we expected to see at least a weakly increasing sensitivity with decreasing wavelength if only at our lowest available wavelengths. This would be expected because defect states in the band gap which could give rise to some absorption would be expected to begin to reflect the character of super band-gap states by radiationless mixing as the energy of the states began to approach the band gap. This is clearly not the case.

4   Report Conclusions

From the beginning of our interest in the tungsten oxide photochromic system we have wondered how sub band-gap excitation could lead to super band-gap chemistry. Energetically, photochromic processes are possible[18] with sub band-gap light but the absorption strength would have seemed to be too small to cause the observed sensitivity. The threshold energy for writing the blue medium compares quite favorably with that measured for other commercial media. We found that using UV light at 385 nm lowered the threshold by a factor of approximately 1000, and adding a layer of TiO_2 lowered the threshold by a factor of 1/3. This suggests that doping and adding other materials could lead to better system performance, and should be investigated.

Given these new measurements, it seems that there are in fact states within the band gap which give rise to weak absorption strength. It is known[20] from many studies of isolated gas phase metal containing species that once a molecule has absorbed a single photon, the absorption of many more, e.g. as many as five or even six, becomes extremely facile. Power indices for these systems rarely reflect the actual number of photons absorbed as now seems apparent in this case.

Given the availability of a myriad of lasers, and the fact that metal oxides are always highly defected materials, it seems reasonable to predict that a variety of processes can be observed and potentially driven for large scale practical utility, which were previously only thought to be significant with super band-gap light. An important example of this would involve catalysis. Currently it is thought that there are defect states associated with each type of binding sites on metal oxide catalysts. Binding of a reactant molecule to a particular binding site is often thought to be the first step in a catalytic cycle. In fact, for tungsten oxide there are thought[21] to be two different types of binding sites. By optically pumping one or the other of these states, perhaps using the wavelengths suggested by Figures 30 and 31, one might be able to selectively activate the associated catalytic processes. These and many other questions would seem to be suggested by the data presented in this report.

5   Appendix A: Labview Data Collection Program

This section contains the documentation for the Labview program used to drive the experimental setup of Section 3.2, Ultraviolet Measurements.   Figure 32 shows the control panel for the experiment, figures 33, 34, and 35 show the graphical program code.

As explained in Section 3.2, the power of the write beam is controlled by a variable neutral density filter and is turned off and on by a shutter, both under computer control. The settings for these are in the upper left-hand block, labeled Power Controller Settings, of the control panel. The start, stop, and step size for rotation of the neutral density filter are specified in degrees. All settings for the shutter must be set manually. The only setting for the shutter is the serial port that it is connected to (com1 or com2). The number of trials at each power level is also set here. The next block down, Translation Stage Settings, specifies how the sample is repositioned between trials as well as the GPIB address of the translation stage controller. The start and stop coordinates set the size of the area that spots are written to, the step size sets the center to center separation of the spots. The power meter GPIB addresses are set in the next block down. The final left-hand block contains the file path where the data is saved, and the parameters written to the data file header. The right hand side of the panel shows the progress of the experiment and the measured powers for the write and read beams.

Figure 32. Virtual Instrument Control Panel

Figure 33 and 34 show the top-level sequence structure for the program. Figure 33 is executed first, setting the shutter port parameters, initializing variables, and creating the data file and its header. Figure 34 shows the body of the program which consists of three nested structures, two FOR loops and a sequence structure. The FOR loops are represented by the square boxes with an N in the upper left hand corner, N being the integer number of times the code inside of the box is executed. The sequence structure is represented by the box that looks like a piece of film. The outer FOR loop sets the write power level, the inner FOR loop conducts the set number of trials at each power level, and the innermost sequence structure runs through the data acquisition sequence for each trial.

The data acquisition sequence is shown in Figure 35. The frames are labeled 0 through 9 at the top of each frame. Frame zero pauses the program for 120 milliseconds. This was necessary to prevent the UDT optical power meter from locking up. Frame 1 instructs the UDT meter to send the current read beam power (the reflected power before writing to the material). Frame 2 starts the GPIB handshaking, allowing the UDT meter to transmit the data. Frame 3 triggers the shutter, exposing the sample to the UV write beam. Frames 4-6 are a repeat of frames 0-2, this time sending the reflected read beam power from the written material. Frame 7 downloads the write beam power from the Newport optical power meter. The commands necessary to do this are executed by the 1830-C sub-vi (virtual instrument). Figure 8 collects the data into a tab delimited line and appends it to the data file. Data is appended after every iteration rather than at the end of a run so that it is not lost if there is a malfunction. Figure 9 contains a virtual instrument that either moves the sample to a new spot or stops the experimental run if there is not any more sample area to write to (the sample area specified and the spot spacing did not allow for enough spots to complete the data run).

Stepping up one level to the inner FOR loop of Figure 34: As was already stated, this loop executes the data collection sequence for the given number of trials at each write power setting. After completion of the loop, the front panel outputs are updated (all readings for a given power level are updated at the same time) and a carriage return is appended to the data file (all data for a given write power appears on one line).

The outermost FOR loop, also in Figure 34, sets a new write power. This is done with the MC-4 sub-vi, which rotates the graded neutral density filter according to the front panel settings. The clock face in the lower right is the sub-vi that calculates the run status.
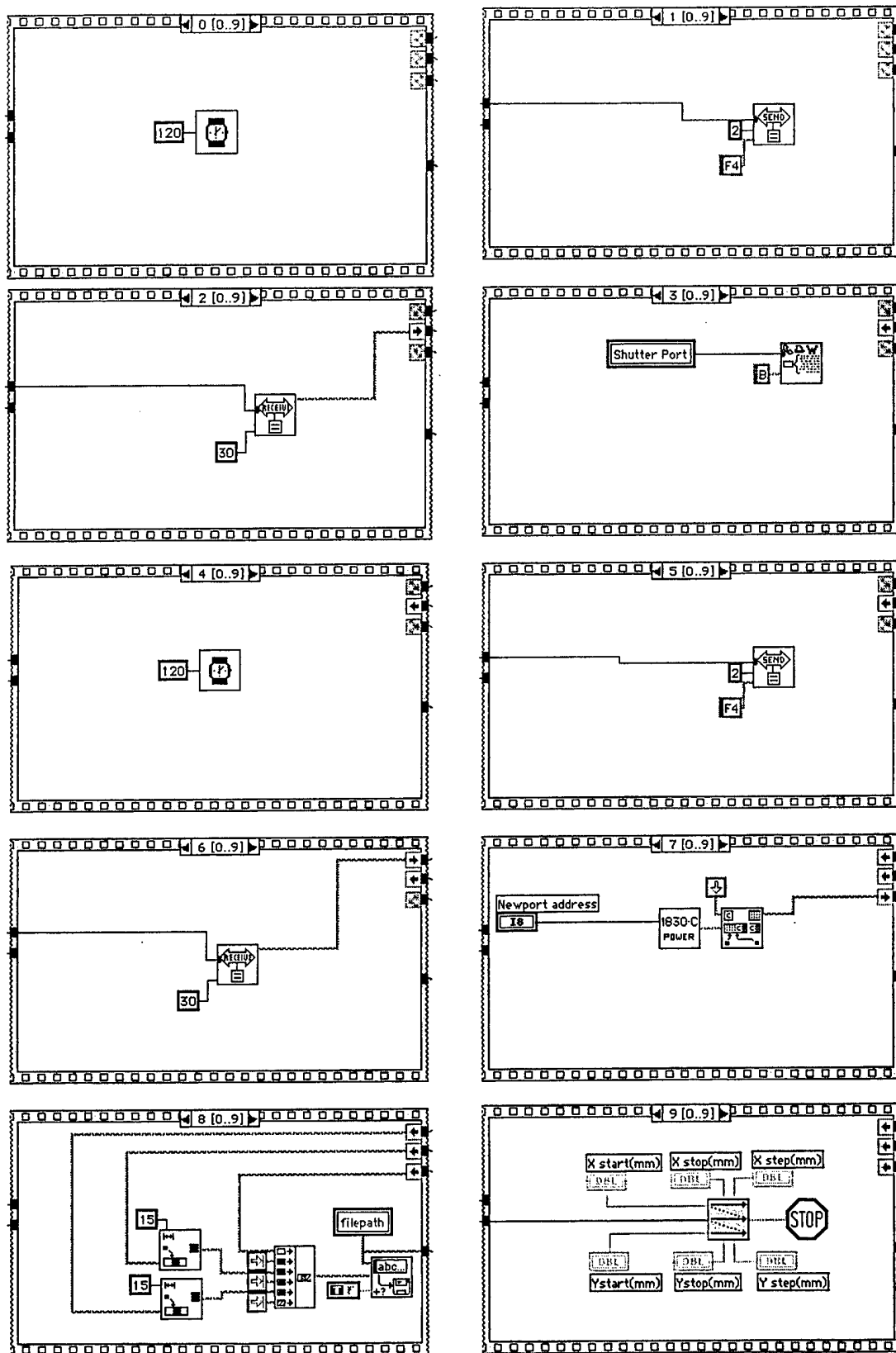
Figure 33. Program and Data File Initializations

Figure 34. Data Collection Section of Program

Figure 35. Data Acquisition Sequence Structure

6 References

1. Osman, J. and Bussjager, R., *Simultaneous Time, Wavelength and Intensity Measurements of Optical Memory Subsystems*, Air Force In-House Report **AFRL-SN-RS-TR-1998-120**

2. Duffy, J.A., *Bonding, Energy Levels and Bands in Inorganic Solids*, p. 185, Longman, 1990.

3. Salje, E., "The Orthorhombic Phase of WO_3", *Acta Cryst.*, **B33**, 574-577, 1977.

4. Cox, P.A., *Transition Metal Oxides*, p. 22, Clarendon Press, Oxford, 1992.

5. Eyring, L. and Tai, L., "The Structural Chemistry of Some Complex Oxides", in Hannay, N.B., *Treatise on Solid State Chemistry Vol. 3*, Plenum, 1976.

6. Iguchi, E. and Tilley, R.J.D., "The Electrostatic Interaction Energy between Crystallographic Shear Planes in Reduced Tungsten Trioxide", *Journ. Solid State Chem.*, **21**, 49-56, 1977.

7. Wells, A.F., *Stuctural Inorganic Chemistry*, p. 571, Clarendon Press, Oxford, 1984.

8. Tilley, R.J.D., "The Crystal Chemistry of the Higher Tungsten Oxides", in Bartha, L. et al., Eds., *The Chemistry of Non-Sag Tungsten*, p. 100, Pergamon, 1995.

9. Cox, P.A., *Transition Metal Oxides*, p. 48, Clarendon Press, Oxford, 1992.

10. Holl, M.M. and Penner-Hahn, J.E., *Chemistry 302 Lecture Summary*, University of Michigan Chemistry Department, on WWW as http://www.umich.edu/~chem302/lectures ummary/wo3/index.html,1997.

11. Berak, J. & Sienko, M., "Effect of Oxygen-Deficiency on Electrical Transport Properties of Tungsten Trioxide Crystals", *Journ. Solid State Chem.*, **2**, 109-133, 1970.

12. Yoshiike, *et al.*, US Patent # 4711815.

* 13. Bussjager, R., *et al.*, *Optical Memory and Interface Systems Final Report*, Air Force In-House Report, **AFRL-SN-RS-TR-1999-81.**

14. Bianchin *et al.* US patent # 4,096,087.

15. Wilson,A., "DVD Technology Increases Image Storage on Rewritable Media", *Vision Systems Design*, pp.52-57, Feb. 1998.

16. A. B. Marchant, *Optical Recording*, p. 45 Addison-Wesley, 1990.

17. Nanolambda Corp. Kerhonksen, NY.

18. Osman, J.M., *et al.*, "Photoredox laser chemistry of transition metal oxides", *Appl. Phys. A.*, **66**, 223-228, 1998.

19. C.G. Granquist, *Handbook of Inorganic Electrochromic Materials*, Elsevier, Amsterdam, 1995. Section 3.3.

20. Chaiken, J., "Conceptual Framework and Overview", Chapter 1 in Chaiken, J. ed., *Laser Chemistry of Organometallics*, ACS Symposium Series, Vol. 530, American Chemical Society, Washington, DC, 1993.

21. Carniti, P., "Energy Distribution of Surface Acid Sites of Metal Oxides", *J. Catal.*, **150**, 274-283, 1994.